The current issue and full text archive of this journal is available on Emerald Insight at:
www.emeraldinsight.com/0332-1649.htm

Dynamic and steady state modeling of permanent magnet induction machine

AQ:au

Hamid Reza Izadfar and Hamid Naseri
Faculty of Electrical and Computer Engineering, Semnan University, Semnan, Iran

Received 21 March 2017
Revised 15 June 2017
Accepted 5 September 2017

Abstract

Purpose – Modeling electric machines is one of the powerful approaches for analyzing their performance. A dynamic model and a steady-state model are introduced for each electric machine. Permanent magnet induction machine (PMIM) is a dual-rotor electric machine, which has various advantages such as high-power factor and low magnetizing current. Studying PMIM and its modeling might be valuable. The purpose of this paper is to introduce a simple and accurate method for dynamic and steady-state modeling of PMIM.

Design/methodology/approach – In this paper, arbitrary dqo reference frame is used to model PMIM. First, three-phase dynamic equations of stator and rotors are introduced. Then, they are transferred to an arbitrary reference frame. The voltage and magnetic flux equations aligned at dqo axes are obtained. These equations give the dynamic model. To investigate the results, PMIM simulation is performed according to obtained dynamic equations. Simulation results verify the analytic calculations.

Findings – In this paper, dynamic equations of PMIM are obtained. These equations are used to determine dynamic equivalent circuits of PMIM. Steady-state equations and one phase equivalent circuit of the PMIM using phasor relations are also extracted.

Originality/value – PMIM equations along dqo axes and their dynamic and steady-state equivalent circuits are determined. These equations and the equivalent circuits can be transformed to different reference frames and analyzed easily.

Keywords Modelling, Equivalent circuit, PMIM, Reference frame, dqo axes

Paper type Research paper

Nomenclature

dqo = the names of axes in a reference frame;
PMIM = permanent magnet induction machine;
PM = permanent magnet;
IM = induction machine; and
MEC = magnetic equivalent circuit.

1. Introduction

Conventional rotational electric machines usually have a stator and a rotor. To enhance power density, performance quality and other output parameters, the number of stators and rotors may be increased. Dual rotor or stator electric machines are machines that are built by combining two similar or dissimilar electric machines. There are different types of combined electric machines such as dual-stator induction machines (Rodrigo *et al.*, 2012; Cheng and Han, 2014), dual-stator winding (Ojo and Wu, 2008), dual-rotor hysteresis motors (Ghanbari *et al.*, 2016), dual-rotor permanent magnet synchronous machines (Zhao *et al.*, 2015), dual-stator permanent magnet synchronous machines (Jiang *et al.*, 2015), dual-rotor switch

COMPEL – The international journal for computation and mathematics in electrical and electronic engineering
Vol. 37 No. 1, 2018
p. 000
© Emerald Publishing Limited
0332-1649
DOI 10.1108/COMPEL-03-2017-0136

reluctance machines (Yang *et al.*, 2016) and dual-rotor induction machines (Cai and Xu, 2014; Sinha *et al.*, 2007).

Permanent magnet induction machine (PMIM) is a dual-rotor electric machine, which is constructed by combining an induction machine with a permanent magnet synchronous machine. It was first introduced in Douglas (1959). Conventional structure of PMIM usually consists of one external stator with three-phase windings, one permanent magnet rotor and one cage (or wounded) induction rotor. Synchronous rotor can supply reactive power of the induction rotor, which reduces inrush current and enhances power factor of the machine (Fukami *et al.*, 2003). PMIM can be used as a motor or a generator. Squirrel cage induction rotor PMIM can be used in constant speed wind turbines, while the wound induction rotor type is useful for variable speed wind turbines. Upon using this machine in wind farms, the instantaneous voltage drop reduces at the starting moment.

For a precise design of PMIM and better utilization, PMIM should be studied in detail. Diao (2015 and Tsuda *et al.* (2007a, 2007b) study how to improve performance of PMIM. Gazdac *et al.* (2013) introduces electric circuit parameters in steady state and discusses control strategy. Operation of PMIM under unbalanced voltage grid conditions has been analyzed by Tsuda *et al.* (2007a, 2007b).

The effects of adding a PM rotor to an induction rotor that constructs a PMIM has been analyzed by Tsuda *et al.* (2007a, 2007b). This paper showed that the energy density of a PMIM is larger than a conventional IM.

Modeling electric machines is one of the powerful approaches for analyzing their performance. Models of electric machines have been extracted based on different approaches such as magnetic equivalent circuit modeling (MEC), dqo dynamic modeling and finite element modeling (FEM). MEC is a powerful approach for real time and non-linear studies of electric machines (Tavana and Dinavahi, 2016). But it cannot represent an electric parameter method. Although FEM produces accurate results, it is very time-consuming, especially for complex systems.The dqo dynamic modeling is an electric equivalent lumped parameter method. It can introduce accurate parametric circuits for dynamic and transient conditions. This method has been used in many studies for modeling electric machines (Piazza *et al.*, 2017; Abdel-Khalik *et al.*, 2016; Tosifian *et al.*, 2012).

For conventional electric machines, the exact dynamic modeling approach has been introduced. PMIM is a combined electric machine, and comprehensive studies on its modeling have not been done so far. In this paper, we present both dynamic and steady state equivalent circuits of PMIM. Although it seems it has been done in some previous studies, there are major differences between the proposed approaches and results.

One of the most famous papers in this context is Fukami *et al.* (2003). This paper introduces the electric equivalent circuit of the PMIM using dual electric and magnetic circuits, where, first, the PM rotor is replaced with a wounded salient pole rotor and then its non-linear equivalent circuit is extracted.

There are two major differences between our results and Fukami *et al.* (2003). First, the introduced equivalent circuit in Fukami *et al.* (2003) is the steady-state equivalent circuit, and it does not discuss dynamic model and behavior of PMIM. Second, unlike this paper, we extract the comprehensive equations of PMIM based on dqo reference frame. AQ: 1

As equations and dynamic equivalent circuit of PMIM are necessary for analyzing its performance, this paper first presents dynamic equations of PMIM for stators and rotors in dqo arbitrary reference frame. Considering appropriate transformation matrices, equations of magnetic fluxes and voltages along q, d and o axes are obtained. By using these equations, dynamic equivalent circuit of this machine in dqo system is determined. Then, the model of PMIM in steady-state conditions is obtained with phasor relations in dqo frame and abc three-phase system. To verify analytical results, a machine with specific parameters is simulated and some of the output parameters are investigated. Simulation results validate the derived equations.

Rest of this paper is organized as follows: Section 2 extracts the dynamic model of PMIM in dqo reference frame. Section 3 analyzes the steady-state conditions of the PMIM and introduces its steady-state model. Section 4 verifies the analytical method through simulation. Finally, Section 5 concludes the paper.

2. Analytic model of permanent magnet induction machine

F1 The selected PMIM has one outer stator and two inner rotors. Figures 1 and 2 show the
F2 selected PMIM structure. There is a set of three phase windings on its slotted stator. Permanent magnet synchronous rotor is located between induction (cage) rotor and stator. Induction rotor is squirrel cage type with bars and rings. In the motor operation mode, rotation direction of both PM and cage rotors are identical.

If the induction rotor's circuit is also considered like stator, with three phase symmetrical windings, voltage equations of stator and induction rotor circuit are as follows. In these equations, the low indices s and r indicate stator and rotor variables, respectively:

$$\boldsymbol{v}_{abcs} = \boldsymbol{r}_s \boldsymbol{i}_{abcs} + p\boldsymbol{\lambda}_{abcs} \tag{1}$$

$$\boldsymbol{v}_{abcr} = \boldsymbol{r}_r \boldsymbol{i}_{abcr} + p\boldsymbol{\lambda}_{abcr} \tag{2}$$

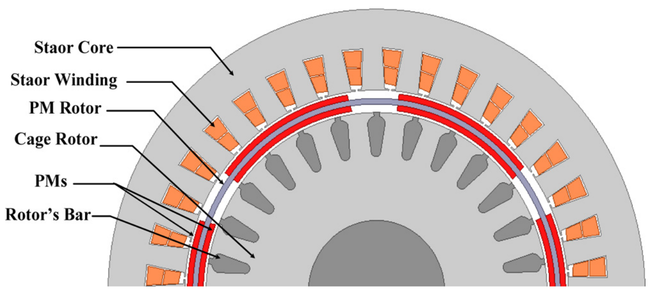

Figure 1. Two-dimensional structure of PMIM

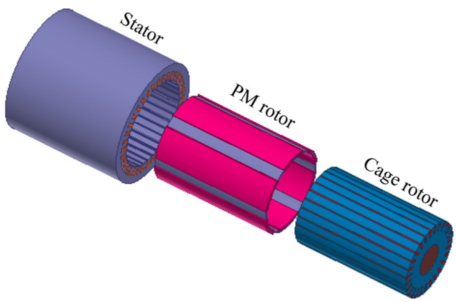

Figure 2. Three-dimensional structure of PMIM

where the stator variables in them are as follows:

$$\boldsymbol{v}_{abcs} = [v_{as}\, v_{bs}\, v_{cs}]^T, \quad \boldsymbol{i}_{abcs} = [i_{as}\, i_{bs}\, i_{cs}]^T, \quad \boldsymbol{\lambda}_{abcs} = [\lambda_{as}\, \lambda_{bs}\, \lambda_{cs}]^T \tag{3}$$

Rotor variables include the following:

$$\boldsymbol{v}_{abcr} = [v_{ar}\, v_{br}\, v_{cr}]^T, \quad \boldsymbol{i}_{abcr} = [i_{ar}\, i_{br}\, i_{cr}]^T, \quad \boldsymbol{\lambda}_{abcr} = [\lambda_{ar}\, \lambda_{br}\, \lambda_{cr}]^T \tag{4}$$

Winding resistance matrix of stator and rotor and introduced as follows:

$$\boldsymbol{r}_s = diag[r_s\, r_s\, r_s], \quad \boldsymbol{r}_r = diag[r_r\, r_r\, r_r] \tag{5}$$

where $\boldsymbol{v}$, $\boldsymbol{i}$ and $\boldsymbol{\lambda}$ are matrices of voltage, current and linkage flux, respectively, and p is the differentiation operator.

Linkage fluxes of the stator and induction rotor are introduced as follows:

$$\boldsymbol{\lambda}_{abcs} = \boldsymbol{\lambda}_{ss} + \boldsymbol{\lambda}_{sr} + \boldsymbol{\lambda}_{sp} \tag{6}$$

$$\boldsymbol{\lambda}_{abcr} = \boldsymbol{\lambda}_{rs} + \boldsymbol{\lambda}_{rr} + \boldsymbol{\lambda}_{rp} \tag{7}$$

$\boldsymbol{\lambda}_{ss}$, $\boldsymbol{\lambda}_{sr}$ and $\boldsymbol{\lambda}_{sp}$ are matrices of linkage flux of the stator produced by stator current, induction rotor and PM synchronous rotor, respectively.

$\boldsymbol{\lambda}_{rs}$, $\boldsymbol{\lambda}_{rr}$ and $\boldsymbol{\lambda}_{rp}$ are also matrices of linkage flux of the induction rotor caused by stator current, current of induction rotor bars and permanent magnets placed on PM rotor, respectively.

To simplify the calculations, following assumptions are considered:

- the saturation is neglected and PMIM is considered as a linear system; and
- magnetic flux distribution of permanent magnets is considered to be a sinusoidal waveform.

With these assumptions, linkage flux matrices are defined as follows:

$$\boldsymbol{\lambda}_{ss} = \boldsymbol{L}_{ss}\boldsymbol{i}_{abcs} \tag{8}$$

$$\boldsymbol{\lambda}_{sr} = \boldsymbol{L}_{sr}\boldsymbol{i}_{abcr} \tag{9}$$

$$\boldsymbol{\lambda}_{rr} = \boldsymbol{L}_{rr}\boldsymbol{i}_{abcr} \tag{10}$$

$$\boldsymbol{\lambda}_{rs} = (\boldsymbol{L}_{sr})^T\boldsymbol{i}_{abcs} \tag{11}$$

$\boldsymbol{L}_{ss}$, $\boldsymbol{L}_{rr}$ and $\boldsymbol{L}_{sr}$ are inductance matrices of stator's windings, rotor windings and mutual inductance matrix, respectively. $(\boldsymbol{L}_{sr})^{\mathbf{T}}$ is the transposed matrix of $\boldsymbol{L}_{sr}$. These matrices are as follows (Krause *et al.*, 2002):

$$\boldsymbol{L}_{ss} = \begin{bmatrix} L_{ls} + L_{ms} & -\dfrac{L_{ms}}{2} & -\dfrac{L_{ms}}{2} \\ -\dfrac{L_{ms}}{2} & L_{ls} + L_{ms} & -\dfrac{L_{ms}}{2} \\ -\dfrac{L_{ms}}{2} & -\dfrac{L_{ms}}{2} & L_{ls} + L_{ms} \end{bmatrix} \tag{12}$$

$$\boldsymbol{L}_{rr} = \begin{bmatrix} L_{lr} + L_{mr} & -\frac{L_{mr}}{2} & -\frac{L_{mr}}{2} \\ -\frac{L_{mr}}{2} & L_{lr} + L_{mr} & -\frac{L_{mr}}{2} \\ -\frac{L_{mr}}{2} & -\frac{L_{mr}}{2} & L_{lr} + L_{mr} \end{bmatrix} \tag{13}$$

$$\boldsymbol{L}_{sr} = L_{sr} \begin{bmatrix} \cos\theta_{ri} & \cos\left(\theta_{ri} + \frac{2\pi}{3}\right) & \cos\left(\theta_{ri} - \frac{2\pi}{3}\right) \\ \cos\left(\theta_{ri} - \frac{2\pi}{3}\right) & \cos\theta_{ri} & \cos\left(\theta_{ri} + \frac{2\pi}{3}\right) \\ \cos\left(\theta_{ri} + \frac{2\pi}{3}\right) & \cos\left(\theta_{ri} - \frac{2\pi}{3}\right) & \cos\theta_{ri} \end{bmatrix} \tag{14}$$

where

$$L_{ms} = \left(\frac{N_s}{2}\right)^2 \frac{\pi \mu_0 r l}{g} \tag{15}$$

$$L_{mr} = \left(\frac{N_r}{2}\right)^2 \frac{\pi \mu_0 r l}{g} \tag{16}$$

$$L_{sr} = \left(\frac{N_s}{2}\right)\left(\frac{N_r}{2}\right) \frac{\pi \mu_0 r l}{g} \tag{17}$$

g, l, r, N_s and N_r are stack length, stator radius, number of winding turns of stator and rotor, respectively, and θ_{ri} is the angular position of the rotor with respect to stator reference axis.

Magnetic flux caused by PM rotor, which links windings of stator and induction rotor, is assumed as a sinusoidal waveform, defined as follows:

$$\boldsymbol{\lambda}_{sp} = \lambda_1 \begin{bmatrix} \sin\theta_{rpm} \\ \sin\left(\theta_{rpm} - \frac{2\pi}{3}\right) \\ \sin\left(\theta_{rpm} + \frac{2\pi}{3}\right) \end{bmatrix} \tag{18}$$

$$\boldsymbol{\lambda}_{rp} = \lambda_2 \begin{bmatrix} \sin(\theta_{rpm} - \theta_{ri}) \\ \sin\left(\theta_{rpm} - \theta_{ri} - \frac{2\pi}{3}\right) \\ \sin\left(\theta_{rpm} - \theta_{ri} + \frac{2\pi}{3}\right) \end{bmatrix} \tag{19}$$

J_ID: COMPEL ART NO: 10.1108/COMPEL-03-2017-0136 Date: 5-December-17 Page: 6 Total Pages: 20 4/Color Figure(s) ARTTYPE="Re

λ_1 and λ_2 are maximum magnitudes of sinusoidal magnetic fluxes, and θ_{rpm} is the angular position of PM rotor with respect to stator reference axis. Usually, variables and components of rotor circuit are transferred to the stator side. New variables of induction rotor would be as follows:

$$i'_{abcr} = \frac{N_r}{N_s}\boldsymbol{i}_{abcr}, \quad v'_{abcr} = \frac{N_s}{N_r}\boldsymbol{v}_{abcr}, \quad \lambda'_{abcr} = \frac{N_s}{N_r}\boldsymbol{\lambda}_{abcr} \tag{20}$$

In addition, the inductance matrices would change as below (Krause *et al.*, 2002):

$$\boldsymbol{L}'_r = \left(\frac{N_s}{N_r}\right)^2 \boldsymbol{L}_r = \begin{bmatrix} L'_{lr} + L_{ms} & -\frac{L_{ms}}{2} & -\frac{L_{ms}}{2} \\ -\frac{L_{ms}}{2} & L'_{lr} + L_{ms} & -\frac{L_{ms}}{2} \\ -\frac{L_{ms}}{2} & -\frac{L_{ms}}{2} & L'_{lr} + L_{ms} \end{bmatrix} \tag{21}$$

$$\boldsymbol{L}'_{sr} = \tfrac{N_s}{N_r}\boldsymbol{L}_{sr} = L_{ms}\begin{bmatrix} \cos\theta_{ri} & \cos\left(\theta_{ri} + \frac{2\pi}{3}\right) & \cos\left(\theta_{ri} - \frac{2\pi}{3}\right) \\ \cos\left(\theta_{ri} - \frac{2\pi}{3}\right) & \cos\theta_{ri} & \cos\left(\theta_{ri} + \frac{2\pi}{3}\right) \\ \cos\left(\theta_{ri} + \frac{2\pi}{3}\right) & \cos\left(\theta_{ri} - \frac{2\pi}{3}\right) & \cos\theta_{ri} \end{bmatrix} \tag{22}$$

2.1 Transforming equations to reference frame

Usually, transferring three-phase symmetrical equations and variables to an appropriate reference frame reduces computation complexity and simplifies the model. In the proposed PMIM, five different reference frames can be defined, and each can be used for modeling. These reference frames are as below:

- stator reference frame is located on the stator and rotates with the speed of $\omega = 0$;
- cage rotor reference frame is located on the induction rotor and rotates with the induction rotor's speed, i.e. $\omega = \omega_{ri}$;
- PM rotor reference frame is located on the PM rotor and rotates with the PM rotor's speed, i.e. $\omega = \omega_{rp}$;
- synchronous reference frame which rotates with synchronous speed, i.e. $\omega = \omega_s$; and
- arbitrary reference frame, which rotates with an undefined speed, i.e. ω.

In this paper, the arbitrary reference frame will be used because the derived equations can be transformed easily to another reference frame by replacing ω with the equivalent speed of reference frame. Appropriate transformations for stator and rotor equations are defined as below:

$$\boldsymbol{f}_{qdos} = \boldsymbol{K}_s \boldsymbol{f}_{abcs} \tag{23}$$

ID: shruti.tavate Time: 13:42 I Path: //mbnas01.cadmus.com/home$/44583$/EM-COMP170136

$$\boldsymbol{f}'_{qdos} = \boldsymbol{K}_r \boldsymbol{f}'_{abcs} \tag{24}$$

In the above equations, f indicates voltage, current or magnetic flux. The transformation matrices are defined as below:

$$\boldsymbol{K}_s = \frac{2}{3}\begin{bmatrix} \cos\theta & \cos\left(\theta - \frac{2\pi}{3}\right) & \cos\left(\theta + \frac{2\pi}{3}\right) \\ \sin\theta & \sin\left(\theta - \frac{2\pi}{3}\right) & \sin\left(\theta + \frac{2\pi}{3}\right) \\ \frac{1}{2} & \frac{1}{2} & \frac{1}{2} \end{bmatrix} \tag{25}$$

$$\boldsymbol{K}_r = \frac{2}{3}\begin{bmatrix} \cos\beta & \cos\left(\beta - \frac{2\pi}{3}\right) & \cos\left(\beta + \frac{2\pi}{3}\right) \\ \sin\beta & \sin\left(\beta - \frac{2\pi}{3}\right) & \sin\left(\beta + \frac{2\pi}{3}\right) \\ \frac{1}{2} & \frac{1}{2} & \frac{1}{2} \end{bmatrix} \tag{26}$$

In the above matrices, θ and β are positions of reference frames with respect to the stator's reference axis, and are defined as follows:

$$\theta = \int_0^t \omega(t)dt + \theta(0) \tag{27}$$

$$\beta = \theta - \theta_{ri} \tag{28}$$

By applying these transformations to equations (1) and (2), following equations are obtained:

$$\boldsymbol{v}_{qdos} = \boldsymbol{K}_s \boldsymbol{r}_s \boldsymbol{K}_s^{-1} \boldsymbol{i}_{qdos} + \left(\boldsymbol{K}_s p \boldsymbol{K}_s^{-1}\right) \boldsymbol{\lambda}_{qdos} + \boldsymbol{K}_s \boldsymbol{K}_s^{-1} (p \boldsymbol{\lambda}_{qdos}) \tag{29}$$

$$v'_{qdor} = \boldsymbol{K}_r r'_r \boldsymbol{K}_r^{-1} i'_{qdor} + \left(\boldsymbol{K}_r p \boldsymbol{K}_r^{-1}\right) \lambda'_{qdor} + \boldsymbol{K}_r \boldsymbol{K}_r^{-1} \left(p \lambda'_{qdor}\right) \tag{30}$$

In a symmetrical three-phase system, the following equations can be proved using trigonometric calculations:

$$\boldsymbol{K}_s \boldsymbol{r}_s \boldsymbol{K}_s^{-1} = \boldsymbol{r}_s \tag{31}$$

$$\boldsymbol{K}_r r'_r \boldsymbol{K}_r^{-1} = r'_r \tag{32}$$

$$\boldsymbol{K}_s p \boldsymbol{K}_s^{-1} = \omega \begin{bmatrix} 0 & 1 & 0 \\ -1 & 0 & 0 \\ 0 & 0 & 0 \end{bmatrix} \tag{33}$$

$$\boldsymbol{K}_r p \boldsymbol{K}_r^{-1} = (\omega - \omega_{ri}) \begin{bmatrix} 0 & 1 & 0 \\ -1 & 0 & 0 \\ 0 & 0 & 0 \end{bmatrix} \tag{34}$$

In linear systems, linkage fluxes $\boldsymbol{\lambda}_{\mathrm{dqos}}$ and $\boldsymbol{\lambda}'_{\mathrm{dqor}}$ can be replaced with multiplication of current and inductance matrices. This is done in the next section.

2.2 Calculations of stator flux linkage

If equation (6) is transferred to the dqo reference frame, stator linkage fluxes are obtained as follows:

$$\boldsymbol{\lambda}_{qdos} = \boldsymbol{K}_s \boldsymbol{L}_{ss} \boldsymbol{K}_s^{-1} \boldsymbol{i}_{qdos} + \boldsymbol{K}_s \boldsymbol{L}_{sr} \boldsymbol{K}_r^{-1} \boldsymbol{i}_{qdor} + \boldsymbol{\lambda}_{sp_{qdos}} \tag{35}$$

$$\boldsymbol{K}_s \boldsymbol{L}_{ss} \boldsymbol{K}_s^{-1} = \begin{bmatrix} L_{is} + \frac{3}{2} L_{ms} & 0 & 0 \\ 0 & L_{is} + \frac{3}{2} L_{ms} & 0 \\ 0 & 0 & L_{is} \end{bmatrix} \tag{36}$$

$$\boldsymbol{K}_s \boldsymbol{L}_{sr} \boldsymbol{K}_r^{-1} = \begin{bmatrix} \frac{3}{2} L_{ms} & 0 & 0 \\ 0 & \frac{3}{2} L_{ms} & 0 \\ 0 & 0 & 0 \end{bmatrix} \tag{37}$$

$$\begin{aligned}
\boldsymbol{\lambda}_{sp_{qdos}} = \boldsymbol{K_s} \boldsymbol{\lambda}_{sp} &= \frac{2}{3}\lambda_1 \begin{bmatrix} \cos\theta & \cos\left(\theta - \frac{2\pi}{3}\right) & \cos\left(\theta + \frac{2\pi}{3}\right) \\ \sin\theta & \sin\left(\theta - \frac{2\pi}{3}\right) & \sin\left(\theta + \frac{2\pi}{3}\right) \\ \frac{1}{2} & \frac{1}{2} & \frac{1}{2} \end{bmatrix} \begin{bmatrix} \sin\theta_{rpm} \\ \sin\left(\theta_{rpm} - \frac{2\pi}{3}\right) \\ \sin\left(\theta_{rpm} + \frac{2\pi}{3}\right) \end{bmatrix} \\
&= \frac{2}{3}\lambda_1 \begin{bmatrix} \cos\theta \ \sin\theta_{rpm} + \cos\left(\theta - \frac{2\pi}{3}\right)\sin\left(\theta_{rpm} - \frac{2\pi}{3}\right) + \cos\left(\theta + \frac{2\pi}{3}\right)\sin\left(\theta_{rpm} + \frac{2\pi}{3}\right) \\ \sin\theta\sin\theta_{rpm} + \sin\left(\theta - \frac{2\pi}{3}\right)\sin\left(\theta_{rpm} - \frac{2\pi}{3}\right) + \sin\left(\theta + \frac{2\pi}{3}\right)\sin\left(\theta_{rpm} + \frac{2\pi}{3}\right) \\ \frac{1}{2}\sin\theta_{rpm} + \frac{1}{2}\sin\left(\theta_{rpm} - \frac{2\pi}{3}\right) + \frac{1}{2}\sin\left(\theta_{rpm} + \frac{2\pi}{3}\right) \end{bmatrix} \\
&= \frac{2}{3}\lambda_1 \begin{bmatrix} -\frac{3}{2}\sin(\theta - \theta_{rpm}) \\ +\frac{3}{2}\cos(\theta - \theta_{rpm}) \\ 0 \end{bmatrix} = \lambda_1 \begin{bmatrix} -\sin(\theta - \theta_{rpm}) \\ \cos(\theta - \theta_{rpm}) \\ 0 \end{bmatrix}
\end{aligned} \tag{38}$$

2.3. Calculations of rotor flux linkage

According to the previous section, and by applying dqo transformations to equation (7), the linkage flux matrix of the rotor in arbitrary reference frame is derived as follows:

$$\lambda'_{qdor} = \boldsymbol{K}_r \left(L'_{sr}\right)^T \boldsymbol{K}_s^{-1} \boldsymbol{i}_{qdos} + \boldsymbol{K}_r L'_r \boldsymbol{K}_r^{-1} i'_{qdor} + \lambda'_{rp_{qdor}} \tag{39}$$

$$\boldsymbol{K}_r \boldsymbol{L}'_r \boldsymbol{K}_r^{-1} = \begin{bmatrix} L'_{lr} + \frac{3}{2}L_{ms} & 0 & 0 \\ 0 & L'_{lr} + \frac{3}{2}L_{ms} & 0 \\ 0 & 0 & L'_{lr} \end{bmatrix} \tag{40}$$

$$\boldsymbol{K}_r \left(L'_{sr}\right)^T \boldsymbol{K}_s^{-1} = \boldsymbol{K}_s \boldsymbol{L}_{sr} \boldsymbol{K}_r^{-1} \tag{41}$$

$$\begin{aligned}
\lambda'_{rp_{qdor}} = \mathbf{K_r}\boldsymbol{\lambda}_{rp} &= \frac{2}{3}\lambda'_2 \begin{bmatrix} \cos\beta & \cos\left(\beta - \frac{2\pi}{3}\right) & \cos\left(\beta + \frac{2\pi}{3}\right) \\ \sin\beta & \sin\left(\beta - \frac{2\pi}{3}\right) & \sin\left(\beta + \frac{2\pi}{3}\right) \\ \frac{1}{2} & \frac{1}{2} & \frac{1}{2} \end{bmatrix} \begin{bmatrix} \sin(\theta_{rpm} - \theta_{ri}) \\ \sin\left(\theta_{rpm} - \theta_{ri} - \frac{2\pi}{3}\right) \\ \sin\left(\theta_{rpm} - \theta_{ri} + \frac{2\pi}{3}\right) \end{bmatrix} \\
&= \frac{2}{3}\lambda'_2 \begin{bmatrix} \cos\beta\sin(\theta_{rpm} - \theta_{ri}) + \cos\left(\beta - \frac{2\pi}{3}\right)\sin\left(\theta_{rpm} - \theta_{ri} - \frac{2\pi}{3}\right) + \cos\left(\beta + \frac{2\pi}{3}\right)\sin\left(\theta_{rpm} - \theta_{ri} + \frac{2\pi}{3}\right) \\ \sin\beta\sin(\theta_{rpm} - \theta_{ri}) + \sin\left(\beta - \frac{2\pi}{3}\right)\sin\left(\theta_{rpm} - \theta_{ri} - \frac{2\pi}{3}\right) + \sin\left(\beta + \frac{2\pi}{3}\right)\sin\left(\theta_{rpm} - \theta_{ri} + \frac{2\pi}{3}\right) \\ \frac{1}{2}\sin(\theta_{rpm} - \theta_{ri}) + \frac{1}{2}\sin\left(\theta_{rpm} - \theta_{ri} - \frac{2\pi}{3}\right) + \frac{1}{2}\sin\left(\theta_{rpm} - \theta_{ri} + \frac{2\pi}{3}\right) \end{bmatrix} \\
&= \frac{2}{3}\lambda'_2 \begin{bmatrix} -\frac{3}{2}\sin(\beta - (\theta_{rpm} - \theta_{ri})) \\ +\frac{3}{2}\cos(\beta - (\theta_{rpm} - \theta_{ri})) \\ 0 \end{bmatrix} = \lambda'_2 \begin{bmatrix} -\sin(\theta - \theta_{rpm}) \\ \cos(\theta - \theta_{rpm}) \\ 0 \end{bmatrix}
\end{aligned} \tag{42}$$

By substituting equations (35) and (41) into equations (29) and (30), dynamic equations of PMIM are obtained. These equations are introduced in the following stator and rotor equations.

Stator equations:

$$v_{qs} = r_s i_{qs} + \omega\lambda_{ds} + p\lambda_{qs} \tag{43}$$

$$v_{ds} = r_s i_{ds} - \omega\lambda_{qs} + p\lambda_{ds} \tag{44}$$

$$v_{0s} = r_s i_{0s} + p\lambda_{0s} \tag{45}$$

$$\lambda_{qs} = L_{ls} i_{qs} + \frac{3}{2}L_{ms}\left(i_{qs} + i'_{qr}\right) - \lambda_1 sin\left(\theta - \theta_{r_{pm}}\right) \tag{46}$$

$$\lambda_{ds} = L_{ls}i_{ds} + \frac{3}{2}L_{ms}\left(i_{ds} + i'_{dr}\right) + \lambda_1 cos\left(\theta - \theta_{r_{pm}}\right) \tag{47}$$

$$\lambda_{0s} = L_{ls}i_{0s} \tag{48}$$

Rotor equations:

$$v'_{qr} = r'_r i'_{qr} + (\omega - \omega_{ri})\lambda'_{dr} + p\lambda'_{qr} \tag{49}$$

$$v'_{dr} = r'_r i'_{dr} - (\omega - \omega_{ri})\lambda'_{qr} + p\lambda'_{dr} \tag{50}$$

$$v'_{0r} = r'_r i'_{0r} + p\lambda'_{0r} \tag{51}$$

$$\lambda'_{qr} = L'_{lr_c} i'_{qr} + \frac{3}{2}L_{ms}\left(i_{qs} + i'_{qr}\right) - \lambda'_2 sin(\theta - \theta_{rpm}) \tag{52}$$

$$\lambda'_{dr} = L'_{lr} i'_{dr} + \frac{3}{2}L_{ms}\left(i_{ds} + i'_{dr}\right) + \lambda'_2 cos(\theta - \theta_{rpm}) \tag{53}$$

$$\lambda'_{0r} = L'_{lr} i'_{0r} \tag{54}$$

According to the above equations, arbitrary equivalent circuit of PMIM is introduced, as in Figures 3 to 5. F3-5

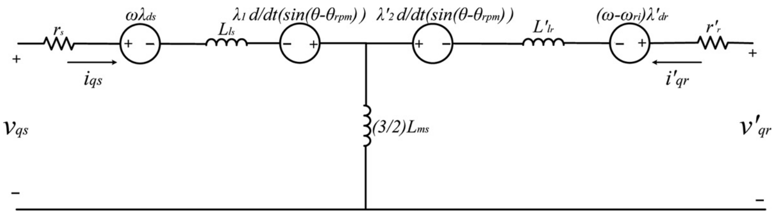

Figure 3.
q axis equivalent circuit of PMIM

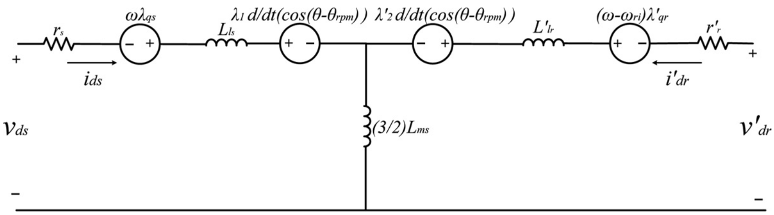

Figure 4.
d axis equivalent circuit of PMIM

3. Analysis of steady state operation and equivalent circuit

Dynamic equivalent circuits obtained in the previous section can be used to analyze performance of the PMIM. A simpler model can be obtained for steady and stable state of this machine. To derive this equivalent circuit, phasor equations in three-phase *abc* system and arbitrary reference frame will be used. In the balanced conditions, zero sequence values of PMIM are zero. d and q quantities have sinusoidal waveform in all reference frames except the synchronous reference frame. In the last reference frame, variables are constant. The sinusoidal steady state variables can be represented with phasors.

For a balanced circuit and in steady state conditions, the phasor representing a and q variables have the following relation (Krause *et al.*, 2002):

$$\overline{F}_a = \overline{F}_q e^{j\theta(0)} \tag{55}$$

If there is no phase shift between a and q axes at $t = 0$, the following relations are established:

$$\overline{F}_{as} = \overline{F}_{qs} \tag{56}$$

$$\overline{F}_{ds} = j\overline{F}_{qs} \tag{57}$$

$$\overline{F'}_{ar} = \overline{F'}_{qr} \tag{58}$$

$$\overline{F'}_{dr} = j\overline{F'}_{qr} \tag{59}$$

In the above equations, $\overline{F}$ indicates phasor of each electric or magnetic variable like voltage, current and flux. Considering equations (45) to (56), voltage and flux phasor relations are written as below. As quantities in the arbitrary reference frame change with frequency $j(\omega_e-\omega)$, this term is used instead of differentiation operation:

$$\overline{V}_{qs} = r_s\overline{I}_{qs} + \omega\overline{\Lambda}_{ds} + j(\omega_e - \omega)\,\overline{\Lambda}_{qs} \tag{60}$$

$$\overline{V'}_{qr} = r_r\overline{I'}_{qr} + (\omega - \omega_r)\overline{\Lambda'}_{dr} + j(\omega_e - \omega)\,\overline{\Lambda'}_{qr} \tag{61}$$

By using equations (58) and (60) in the above relations, and after a few simplifications, we have the following:

$$\overline{V}_{qs} = r_s\overline{I}_{qs} + j\omega_e\,\overline{\Lambda}_{qs} \tag{62}$$

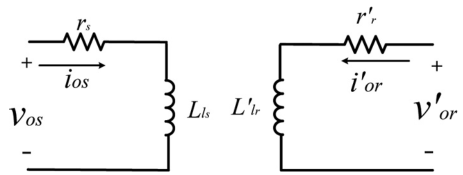

Figure 5.
o axis equivalent circuits of PMIM

J_ID: COMPEL ART NO: 10.1108/COMPEL-03-2017-0136 Date: 5-December-17 Page: 12 Total Pages: 20 4/Color Figure(s) ARTTYPE="R

$$\overline{V'}_{qr} = r'_r \overline{I'}_{qr} + j(\omega_e - \omega_r)\overline{\Lambda'}_{qr} \tag{63}$$

$$\overline{\Lambda}_{qs} = \frac{X_{ls}}{\omega_b}\overline{I}_{qs} + \frac{X_M}{\omega_b}\left(\overline{I}_{qs} + \overline{I}'_{qr}\right) - \lambda_1 e^{-j\theta_{rpm}} \tag{64}$$

$$\overline{\Lambda'}_{qr} = \frac{X'_{lr}}{\omega_b}\overline{I'}_{qr} + \frac{X_M}{\omega_b}\left(\overline{I}_{qs} + \overline{I'}_{qr}\right) - \lambda'_2 e^{-j\theta_{rpm}} \tag{65}$$

By substituting equations (65) and (66) into equations (63) and (64), and after manual calculations, the following equations can be derived:

$$\overline{V}_{qs} = \left(r_s + j\frac{\omega_e}{\omega_b}X_{ls}\right)\overline{I}_{qs} + j\frac{\omega_e}{\omega_b}X_M\left(\overline{I}_{qs} + \overline{I}'_{qr}\right) - \lambda_1\omega_e e^{-j\theta_{rpm}} \tag{66}$$

$$\overline{V'}_{qr} = \left(r'_r + j\frac{\omega_e - \omega_r}{\omega_b}X'_{lr}\right)\overline{I}'_{qr} + j\frac{\omega_e - \omega_r}{\omega_b}X_M\left(\overline{I}_{qs} + \overline{I}'_{qr}\right) - j(\omega_e - \omega_r)\lambda'_2 e^{-j\theta_{rpm}} \tag{67}$$

Now, three-phase equations of stator and rotor voltages can be derived using equations (57) and (59). Considering slip definition as below:

$$s = \frac{\omega_e - \omega_r}{\omega_e} \tag{68}$$

Three-phase equations of PMIM in the steady state conditions can be obtained as follows:

$$\overline{V}_{as} = \left(r_s + j\frac{\omega_e}{\omega_b}X_{ls}\right)\overline{I}_{as} + j\frac{\omega_e}{\omega_b}X_M\left(\overline{I}_{as} + \overline{I}'_{ar}\right) - j\lambda_1\omega_e e^{-j\theta_{rpm}} \tag{69}$$

$$\frac{\overline{V'}_{ar}}{s} = \left(\frac{r'_r}{s} + j\frac{\omega_e}{\omega_b}X'_{lr}\right)\overline{I}'_{ar} + j\frac{\omega_e}{\omega_b}X_M\left(\overline{I}_{as} + \overline{I}'_{ar}\right) - j\omega_e\lambda'_2 e^{-j\theta_{rpm}} \tag{70}$$

Steady state equivalent circuit of PMIM for phase *a* according to equations (70) and (71) is shown in Figure 6. F6

If $\lambda_1 = \lambda'_2 = \lambda$, steady state equivalent circuit can be simplified as Figure 7. In the normal operation, terminals of induction rotor are short circuit. This equivalent circuit is F7

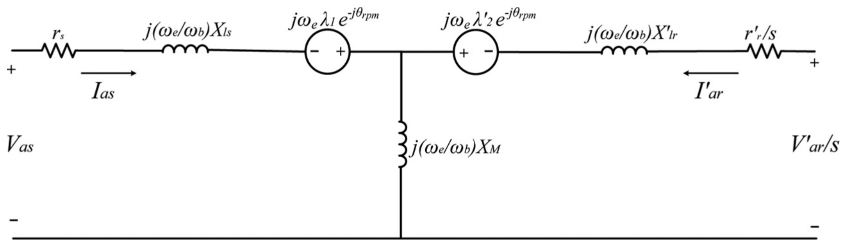

Figure 6.
One phase steady state equivalent circuit of PMIM

ID: shruti.tavate Time: 13:43 I Path: //mbnas01.cadmus.com/home$/44583$/EM-COMP170136

very similar to induction machine's circuit. The difference is the dependent voltage source in parallel branch that is produced because of the PM rotor.

4. Validating the model

In this section, one specified PMIM is simulated on the basis of the dynamic equations and circuit obtained in previous sections and its main parameters are examined. Specifications of
T1 the proposed PMIM are presented in Table I. Figure 8 shows flowchart of the simulation
F8 procedure. Simulation is done on symmetrical and balanced conditions.

Value of inductances of stator windings, rotor bars and mutual inductances are calculated on the basis of the winding function theory and based on the method introduced in Muñoz and Lipo (1999).

Currents and linkage fluxes are calculated according to equations (45) to (56). Note that differentiation operator usually slows down computations and reduces stability margin. Thus, it is better to modify these equations and use integral operator for simulation.

F9 Figure 9 shows current of one phase stator. This current could reach to its rated value.
F10 Speed variations of both rotors are shown in Figure 10. Speed of PM rotor reaches to its nominal speed, i.e. 1,000 rpm, while induction rotor will rotate with a lower speed because of slip phenomenon. The amplitude of speed oscillations of PM rotor is much smaller than the

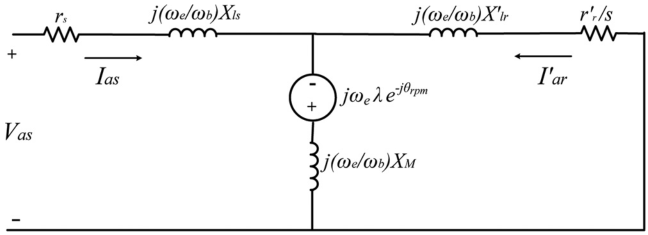

Figure 7.
Simplified equivalent circuit of PMIM

Parameter	Value
Stator outer diameter (mm)	200
Stator inner diameter (mm)	142
Number of stator slots	36
Number of rotor slots	27
Stack length (mm)	135
PM rotor outer diameter (mm)	141
Cage rotor outer diameter (mm)	127
Magnet height (mm)	2
Air gap length (mm)	0.5
Output power (KW)	6
Rated current (A)	8.6
Rated voltage (v)	230
Cage-rated speed (rpm)	920
PM rotor-rated speed (rpm)	1,000
Number of pole pairs	3
Moment of inertia PM rotor (kg/m^2)	0.01
Moment of inertia cage rotor (kg/m^2)	0.04

Source: Gazdac *et al.* (2013)

Table I.
Specifications of simulated PMIM

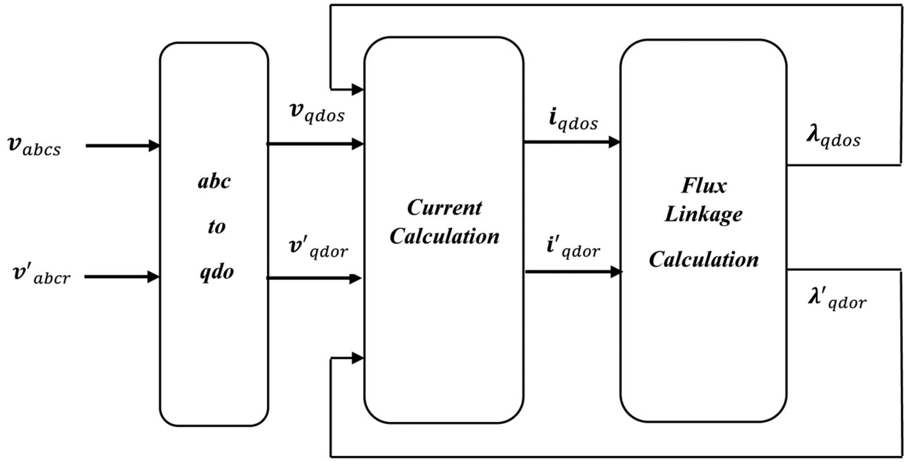

Figure 8.
Flowchart for simulation of PMIM

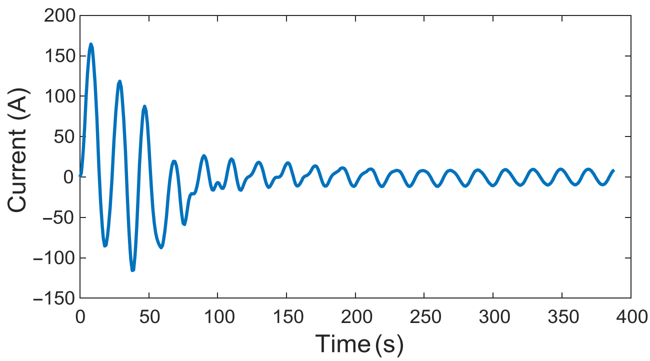

Figure 9.
Stator current waveform

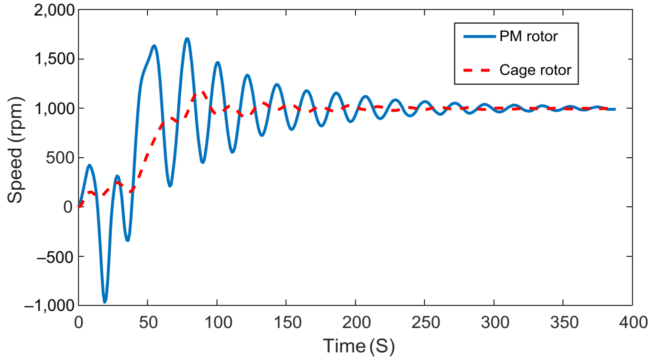

Figure 10.
Speed variations of rotors

J_ID: COMPEL ART NO: 10.1108/COMPEL-03-2017-0136 Date: 5-December-17 Page: 15 Total Pages: 20 4/Color Figure(s) ARTTYPE="R

F11 cage rotor in both dynamic and steady state conditions. Figure 11 shows electromagnetic torques produced by PM and induction rotors. In the motor operation mode, both rotors can produce output mechanical energy. As expected, PM rotor produces an electromagnetic torque with lower ripple.

Speed variations of both rotors after a sudden change in load torque are shown in
F12 Figure 12. At time t1, a step-up variation occurred for load torque of PM rotor. As can be seen in this figure, both rotors are immediately transferred to new operating point. This
F13 analysis has been repeated for cage rotor. As seen in Figure 13, at time t2, the load of cage rotor has increased as a step up, while the load of PM rotor remained constant. This figure shows that PMIM has reliable and satisfied operation under these conditions.

5. Finite element analysis

It is essential that the simulation results should be validated. For this purpose, finite element
F14 analysis method was used. The Maxwell software was also used for FEM modeling and
F15 calculation. Figure 14 shows the solved PMIM with Maxwell software. Speed variation of
F16 PM rotor can be seen in Figure 15. Figure 16 shows the speed of cage rotor with two
F17 different methods. Also, comparison of the electromagnetic torques is depicted in Figures 17
F18 and 18.

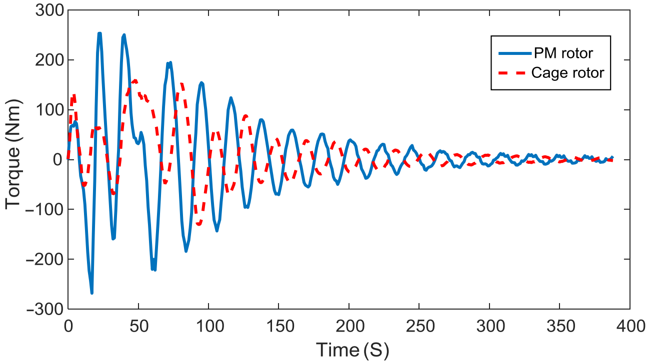

Figure 11.
Electromagnetic torque variations of rotors

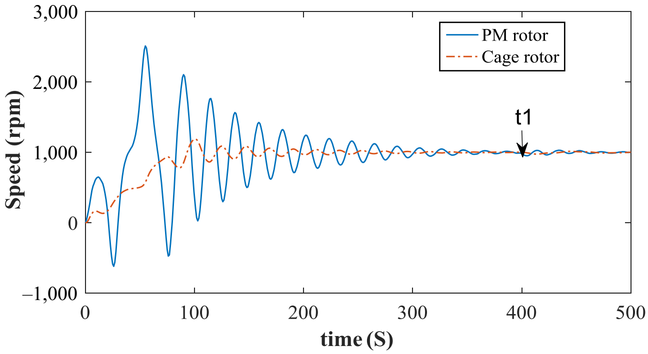

Figure 12.
Variations of speed in step-up change of PM rotor load

ID: shruti.tavate Time: 13:43 I Path: //mbnas01.cadmus.com/home$/44583$/EM-COMP170136

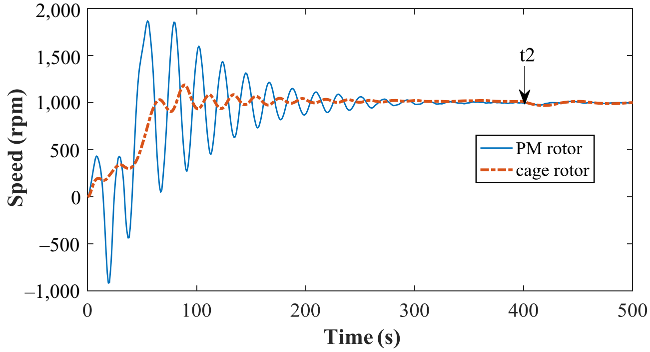

Figure 13.
Variations of speed in step-up change of cage rotor load

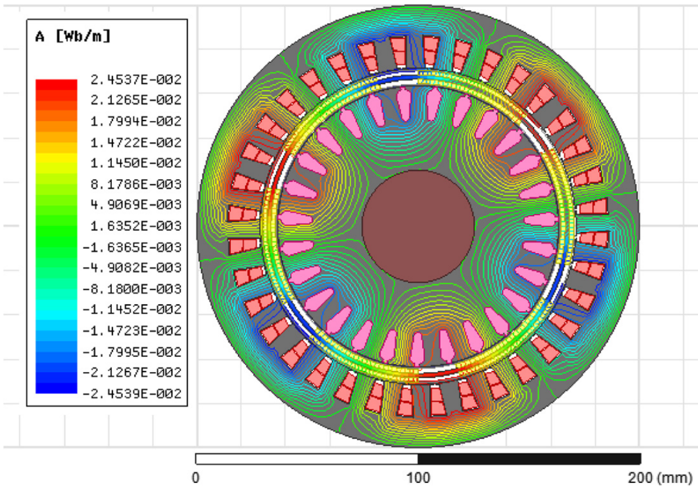

Figure 14.
FE analysis of PMIM

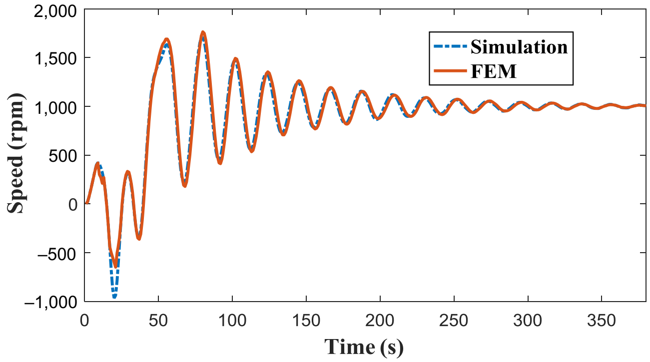

Figure 15.
Speed variations of PM rotor

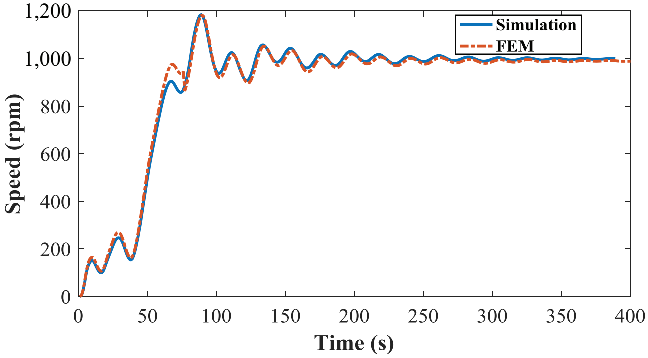

Figure 16.
Speed variations of cage rotor

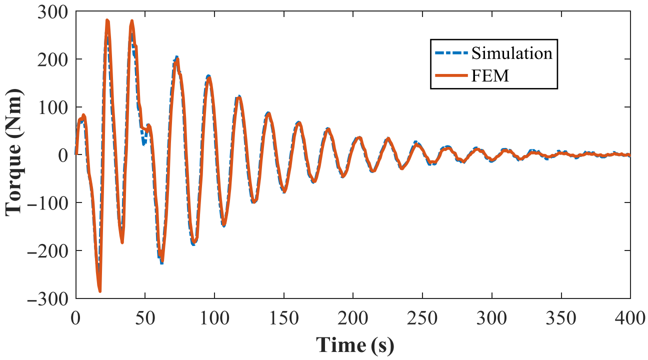

Figure 17.
Electromagnetic torque of PM rotor

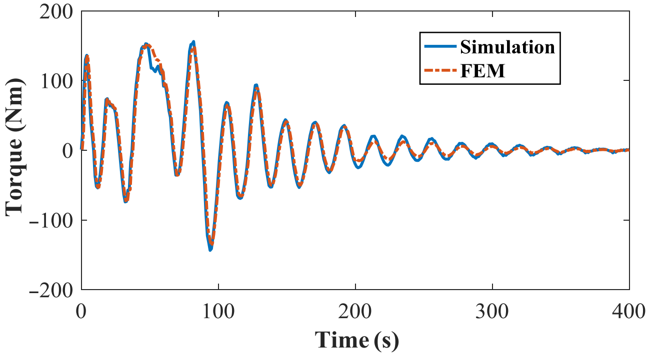

Figure 18.
Electromagnetic torque of cage rotor

6. Conclusion

In this paper, dynamic equations and dqo reference frame equivalent circuits of PMIM have been extracted. These equations can be used to analyze performance and simulation of this machine. After derivation of dynamic model, steady-state operation and equivalent circuit of

PMIM is also derived. To this end, the relation between phasors of three-phase and dqo components is used. At the end, simulation flowchart is introduced and a specific PMIM is simulated using the derived dynamic equations.

References

Abdel-Khalik, A., Ahmed, S. and Ahmed, M. (2016), "Dynamic modeling of a five-phase induction machine with a combined star/pentagon stator winding connection", *IEEE Transactions on Energy Conversion*, Vol. 31 No. 4, doi: 10.1109/TEC.2016.2565819.

Cai, H. and Xu, L. (2014), "Modeling and control for cage rotor dual mechanical port electric machine—Part II: independent control of two rotors", *IEEE Transactions on Energy Conversion*, Vol. 30 No. 3, pp. 966-973.

Cheng, M. and Han, P. (2014), "A dual-stator brushless doubly-fed induction motor for EV/HEV applications", *International Conference on Intelligent Green Building and Smart Grid (IGBSG), Taipei*, pp. 23-25.

Diao, T. (2015), "Study on dual-rotor permanent magnet induction motor and performance", *The Open Electrical & Electronic Engineering Journal*, Vol. 9 No. 1, pp. 584-590.

Douglas, J.F.H. (1959), "Characteristics of induction motors with permanent magnet excitation", *Transactions of the American Institute of Electrical Engineers: Part III: Power Apparatus and Systems*, Vol. 78 No. 3, pp. 221-225.

Fukami, T., Nakagawa, K., Hanaoka, R., Takata, S. and Miyamoto, T. (2003), "Nonlinear modeling of a permanent-magnet induction machine", *Electrical Engineering in Japan*, Vol. 144 No. 1, pp. 58-67.

Gazdac, A., Di Leonardo, L., Mabwe, A., Betin, F. and Illani, M. (2013), "Electric circuit parameters identification and control strategy of dual-rotor permanent magnet induction machine", *IEEE International on Electric Machines & Drives Conference (IEMDC), Chicago, IL*, pp. 1102-1107.

Ghanbari, T., Sanati Moghadam, M. and Darabi, A. (2016), "Comparison between coreless and slotless kinds of dual rotor discs hysteresis motors", *IET Electric Power Applications*, Vol. 10 No. 2, pp. 133-140.

Jiang, X., Huang, W. and Cao, R. (2015), "Analysis of a dual-winding fault-tolerant permanent magnet machine drive for aerospace applications", *IEEE Transactions on Magnetics*, Vol. 51 No. 11, doi: 10.1109/TMAG.2015.2457775.

Krause, P.C., Wasynczuk, O. and Sudhoff, S.D. (2002), *Analysis of Electric Machinary and Drive Systems*, 2nd ed., Wiely Inter Science, Hoboken, NJ.

Muñoz, A.R. and Lipo, T.A. (1999), "Complex vector model of the squirrel-cage induction machine including instantaneous rotor Bar currents", *IEEE Transaction on Industry Applications*, Vol. 35 No. 6, pp. 57-64.

Ojo, O. and Wu, Z. (2008), "Modeling of a dual-stator-winding induction machine including the effect of main flux linkage magnetic saturation", *IEEE Transaction on Industry Applications*, Vol. 44 No. 4.

Piazza, M., Luna, M. and Pucci, M. (2017), "Electrical loss minimization technique for wind generators based on a comprehensive dynamic modelling of induction machines", *IEEE Transaction on Industry Applications*, Vol. 53 No. 4, doi: 10.1109/TIA.2017.2691307.

Rodrigo, J., Puig, X., Blavi, H. and Pesquer, L. (2012), "Implementation, modelling and performance analysis of a dual stator-winding induction generator", *The International Journal for Computation and Mathematics in Electrical and Electronic Engineering (COMPEL)*, Vol. 32 No. 1, pp. 302-312.

Sinha, S., Deb, N. and Mondal, N. (2007), "Design and performance of single stator, dual rotor induction motor", *International Conference on Power Electronics and Drive Systems, Bangkok*, November 2007, pp. 1163-1166.

Tavana, N. and Dinavahi, V. (2016), "Real-time nonlinear magnetic equivalent circuit model of induction machine on FPGA for hardware-in-the-loop simulation", *IEEE Transactions on Energy Conversion*, Vol. 31 No. 2, pp. 520-530.

Tosifian, M., Nazarzadeh, J. and Abedi, M. (2012), "A new dynamical model of linear induction machines", *Electric Power Components and Systems*, Vol. 40 No. 11, pp. 1319-1338.

Tsuda, T., Fukami, T., Kanamaru, Y. and Miyamoto, T. (2007a), "Performance analysis of the permanent-magnet induction generator under unbalanced grid voltages", *Electrical Engineering in Japan*, Vol. 161 No. 4, pp. 1126-1133.

Tsuda, T., Fukami, T., Kanamaru, Y. and Miyamoto, T. (2007b), "Effects of the built-in permanent magnet rotor on the equivalent circuit parameters of a permanent magnet induction generator", *IEEE Transactions on Energy Conversion*, Vol. 22 No. 3, pp. 798-799.

Yang, Y., Schofield, N. and Emadi, A. (2016), "Double-rotor switched reluctance machine design, simulations, and validations", *IET Electrical Systems in Transportation*, Vol. 6 No. 2, pp. 117-125, doi: 10.1049/iet-est.2015.0028.

Zhao, W., Lipo, T.A. and Kwon, B. (2015), "A novel dual-rotor, axial field, fault-tolerant flux-switching permanent magnet machine with high-torque performance", *IEEE Transactions on Magnetics*, Vol. 51 No. 11, doi: 10.1109/TMAG.2015.2445926.

Corresponding author
Hamid Reza Izadfar can be contacted at: hrizadfar@semnan.ac.ir

For instructions on how to order reprints of this article, please visit our website:
www.emeraldgrouppublishing.com/licensing/reprints.htm
Or contact us for further details: **permissions@emeraldinsight.com**

AUTHOR QUERIES

AUTHOR PLEASE ANSWER ALL QUERIES

AQau— Please confirm the given-names and surnames are identified properly by the colours.
=Given-Name, = Surname
The colours are for proofing purposes only. The colours will not appear online or in print.

AQ1— Please check the edits made in the following sentence, and correct if necessary: There are two major differences between our results and Fukami *et al.* (2003).